KAP, the Accessory Subunit of Kinesin-2, Binds the Predicted Coiled-Coil Stalk of the Motor Subunits †

ARTICLE *in* BIOCHEMISTRY · FEBRUARY 2009

Impact Factor: 3.02 · DOI: 10.1021/bi8018338 · Source: PubMed

8 AUTHORS, INCLUDING:

Debnath Ghosal
University of Cambridge
6 PUBLICATIONS **26** CITATIONS
SEE PROFILE

Anirban Bhaduri
Samsung Advanced Institute of Technology
18 PUBLICATIONS **177** CITATIONS
SEE PROFILE

Ramanathan Sowdhamini
Tata Institute of Fundamental Research
219 PUBLICATIONS **2,589** CITATIONS
SEE PROFILE

Krishanu Ray
Tata Institute of Fundamental Research
34 PUBLICATIONS **843** CITATIONS
SEE PROFILE

KAP, the Accessory Subunit of Kinesin-2, Binds the Predicted Coiled-Coil Stalk of the Motor Subunits[†]

Harinath Doodhi,[‡,§] Debnath Ghosal,[‡,§] Mahalakshmi Krishnamurthy,[‡,§] Swadhin C. Jana,[‡] Divya Shamala,[||] Anirban Bhaduri,[||] R. Sowdhamini,[||] and Krishanu Ray*[,‡]

Tata Institute of Fundamental Research, Homi Bhabha Road, Colaba, Mumbai 400005, India, and National Center for Biological Sciences, Bangalore 560065, India

Received September 28, 2008; Revised Manuscript Received January 21, 2009

ABSTRACT: Kinesin-2 is an anterograde motor involved in intraflagellar transport and certain other intracellular transport processes. It consists of two different motor subunits and an accessory protein KAP (kinesin accessory protein). The motor subunits were shown to bind each other through the coiled-coil stalk domains, while KAP was proposed to bind the tail domains of the motor subunits. Although several genetic studies established that KAP plays an important role in kinesin-2 functions, its exact role remains unclear. Here, we report the results of a systematic analysis of the KAP binding sites by using recombinant *Drosophila* kinesin-2 subunits as well as the endogenous proteins. These show that at least one of the coiled-coil stalks is sufficient to bind the N-terminal region of DmKAP. The soluble complex involving the recombinant kinesin-2 fragments is reconstituted in vitro at high salt concentrations, suggesting that the interaction is primarily nonionic. Furthermore, independent distant homology modeling indicated that DmKAP may bind along the coiled-coil stalks through a combination of predominantly hydrophobic interactions and hydrogen bonds. These observations led us to propose that KAP would stabilize the motor subunit heterodimer and help assemble a greater kinesin-2 complex in vivo.

Kinesin-2 is a member of the kinesin superfamily of microtubule (MT)[1] dependent motor proteins. It is a heterotrimeric complex of three dissimilar subunits. The holoenzyme, as purified from sea urchin embryos, is an equal molar complex of two different motor subunits and a larger nonmotor accessory protein KAP (*1, 2*). Orthologues of the motor subunits as well as the accessory proteins are identified in several different organisms, including humans (*3*). Kinesin-2 propels anterograde intraflagellar transport (IFT) into the flagella and cilia of a variety of cells (*4, 5*), and loss of kinesin-2 gene functions is shown to block the formation of primary cilia in mouse embryos (*3, 6*−*8*). It is also implicated in certain chronic human disorders such as Bardet-Biedl syndrome (*9*) and polycystic kidney disease (*10*). KLP64D, KLP68D, and DmKAP constitute the *Drosophila* kinesin-2 (*11*−*13*). Mutations in the *Klp64D* gene affect the anterograde axonal transports of choline acetyltransferase (ChAT) and acetylcholinesterase (AChE) (*12, 14*), and mutations in the *DmKap* gene as well as in the *Klp64D* gene block the formation of sensory cilia in chordotonal neurons (*13*). All these indicate that kinesin-2 is a versatile motor involved in multiple different transports involving a large variety of cargoes.

Results of genetic interaction studies suggest that KAP plays an important role in kinesin-2 functions in vivo. In *Chlamydomonas*, *fla10* and *fla3* encode a kinesin-2 motor subunit and the accessory protein, respectively (*5*). Mutations in both these genes are shown to cause similar losses of the anterograde IFT and flagella resorption (*15, 16*), and the FLA10 protein is shown to accumulate at the transition zone near the basal body in the *fla3-1* mutant (*16*). In *Drosophila*, mutation in the *DmKap* gene is shown to eliminate the sensory cilia of the chordotonal neurons and impair auditory reception by the Johnston's organ in the adult antennae (*13*). It also dominantly enhanced the partial loss of function defect in the *Klp64D* homozygous mutant background (*13*). Simi-

[†] This work has been supported by the intramural funds of the Tata Institute of Fundamental Research and DST Grant SR/SO/BB-59/2006 to K.R.

* To whom correspondence should be addressed: Tata Institute of Fundamental Research, Homi Bhabha Road, Mumbai 400005, India. Phone: 91-22-22782730. Fax: 91-22-22804610/11. E-mail: krishanu@tifr.res.in.

[‡] Tata Institute of Fundamental Research.

[§] These authors contributed equally to this work.

[||] National Center for Biological Sciences.

[1] Abbreviations: MT, microtubule; IFT, intraflagellar transport; ChAT, choline acetyltransferase; AChE, acetylcholinesterase; KLP64D, kinesin-like protein 64D; KLP68D, kinesin-like protein 68D; DmKAP, *Drosophila melanogaster* kinesin accessory protein; MmKAP3A, *Mus musculus* KAP; MmKIF3A/B, *M. musculus* kinesin-like protein 3A and 3B heterodimer; XKLP3A, *Xenopus* kinesin-like protein 3A; XKLP3B, *Xenopus* kinesin-like protein 3B; XKAP, *Xenopus* KAP; SpKRP85, *Strongylocentrotus purpuratus* kinesin-related protein of 85 kDa; SpKRP95, *S. purpuratus* kinesin-related protein of 95 kDa; SpKAP115, *S. purputarus* KAP of 115 kDa; Fw, formula weight; M_r, molecular mass; His, hexahistidine tag; GST, glutathione *S*-transferase; IPTG, isopropyl thiogalactoside; DTT, dithiothreitol; mAb, monoclonal antibody; HRP, horseradish peroxidase; SDS, sodium dodecyl sulfate; PAGE, polyacrylamide gel electrophoresis; S, stalk fragment; T, tail domain; KLP64DS, KLP64D stalk fragment; KLP68DS, KLP68D stalk fragment; KLP64D/68DS, heterodimer of KLP64D and KLP68D stalks; KLP64DT, KLP64D tail fragment; KLP68DT, KLP68D tail fragment; KLP64D1/3ST, KLP64D one-third stalk with the tail fragment; KLP68D1/3ST, KLP68D one-third stalk with the tail fragment; KHC, kinesin heavy chain; GFP, green fluorescent protein; *Pf*PFK, *Plasmodium falciparum* phosphofructokinase; ARM, armadillo-like repeat motif.

10.1021/bi8018338 CCC: $40.75
Published on Web 01/22/2009

larly, mutations in the *Caenorhabditis elegans* KAP are shown to affect the kinesin-2-mediated transport into the sensory cilia (*17*). In contrast, studies with recombinant MmKIF3A/B and MmKAP3A suggested that the accessory protein has no role in kinesin-2 motor activity in vitro (*18*). Hence, the exact role of KAP in the kinesin-2 function is still unclear.

Understanding the mechanisms of subunit assembly can provide clues about their functions in a complex. Studies with the mouse (MmKIF3A and MmKIF3B) and *Xenopus* (XKLP3A and XKLP3B) homologues of the kinesin-2 motor subunits revealed that they can form a heterodimer only through coiled-coil interactions between the stalk domains at the middle (*19, 20*). These studies also showed that the two subunits must be coexpressed for this purpose and the coiled-coil domain of the XKLP3A is required to fold the XKLP3B stalk around it (*21*). These suggested that the heterodimerization is essential for formation of a functional kinesin-2 motor. The recombinant MmKAP3A subunit was shown to bind the MmKIF3A/B heterodimer in vitro (*18*), and studies with both SpKAP115 of sea urchin and MmKAP3A suggested that they could bind the C-terminal tail domains of the kinesin-2 motor subunits in the respective organisms (*2, 18*). However, a lack of KAP binding reportedly did not change the MT gliding activity of the recombinant motor duplex (*18*). On the basis of these observations, it was suggested that KAP would function as a cargo adapter for kinesin-2. The evidence was, however, mainly derived from electron microscopic observations, and though the KAP was proposed to bind the tail domains through complementary charge interactions, the heterotrimeric kinesin-2 holoenzyme was demonstrated to remain stable even at 500 mM KCl (*2*). This resulted in confusion about the exact nature and region of interaction between the KAP and the motor subunits.

To resolve these issues, we attempted to map the interactions between the KAP and the motor subunits using the *Drosophila* kinesin-2 homologues. Fragments of DmKAP, KLP64D and KLP68D, were cloned and expressed in *Escherichia coli* with affinity tags, which were then used to copurify the native subunits by affinity chromatography. Contrary to the current belief, our studies revealed that the N-terminal region of DmKAP could bind directly to the predicted stalk fragments of the motor subunits. The interaction is stable at very high ionic concentrations. Furthermore, distant homology modeling studies and molecular docking analysis suggested that DmKAP could simultaneously associate with the predicted coiled-coil domains of both the KLP64D and KLP68D fragments through a combination of hydrophobic and charge interactions. On the basis of these results, we propose a new role for KAP in kinesin-2 assembly and function in this report.

MATERIALS AND METHODS

Recombinant DNA and Protein Purification Methods. Fragments were PCR amplified from the full-length cDNA clones of KLP64D (Fw = 76230.6), KLP68D (Fw = 88607.4), and DmKAP (Fw = 116759.1) and subcloned into suitable expression vectors. The subcloning details and the vectors are provided in Table 1 of the Supporting Information. A majority of the recombinant fragments were cloned into the pET series vectors with an N-terminal hexahistidine (His) tag. Only two of the DmKAP fragments were cloned in the pGEX4T vector downstream of an N-terminal glutathione *S*-transferase (GST) tag (see Figures 2A and 3A and Table 1 of the Supporting Information for details). The cloned DNA plasmids were separately transformed into *E. coli* BL21(DE3) cells. The log-phase suspension cultures of these transformed *E. coli* cells were induced with 0.5 mM IPTG for 4 h at 28 °C as described previously (*22*). Subsequently, the bacterial cells were harvested at 8000*g* and resuspended in lysis buffer [20 mM HEPES (pH 7.4), 40 mM KCl, 5 mM $MgSO_4$, 10 mM EGTA, 10 mM aspartate, 1 mM DTT, 20 mM imidazole, 1 mM PMSF, and 1% Triton X-100] containing 0.5 mg/mL lysozyme and tablets of protease inhibitor cocktail (Roche GmBH, catalog no. 11836170001). Ten milliliter of lysis buffer was used to resuspend 1 g of cell pellet in each case. The cell suspension was sonicated briefly on ice to disrupt the cells and then cleared by centrifugation at 4 °C for 45 min at 70000*g*. The recombinant proteins were then purified from the supernatants by using Ni-NTA agarose (Qiagen Inc.) or glutathione Sepharose (GE Healthcare Ltd.) beads as per the manufacturer's protocols. For some experiments, the affinity-purified proteins were further separated by gel filtration chromatography (column, Superdex-75; AKTA FPLC machine, GE Healthcare Ltd.) in TMN-D (20 mM Tris-HCl, 5 mM $MgCl_2$, 250 mM NaCl, and 1 mM DTT). The peak protein fractions were then concentrated by using Centricon spin concentrators [Millipore (India) Ltd.], and the buffers were exchanged by using a PD-10 desalting column (GE Healthcare Ltd.) as per the supplier's protocol. The quality of the purified recombinant proteins was assessed in Coomassie-stained SDS−PAGE gels at every step, and the protein concentrations were separately estimated with a Bradford assay (reagent obtained from BioRad Plc.) and by spectrophotometric absorption (280 nm).

Drosophila Head Extracts. Approximately 100 fly heads were manually separated by razor blades and homogenized in 250 μL of ice-cold high-KCl buffer [19 mM KH_2PO_4, 81 mM K_2HPO_4, 400 mM KCl, and 1 mM DTT (pH 7.4)] containing the protease inhibitor cocktail (Roche GmbH). A motorized plastic homogenizer and specially designed microfuge tubes were used for this purpose (Pellet Pestle). The homogenate was first centrifuged at 17000*g* for 30 min in a refrigerated microcentrifuge (Biofuge *Fresco*, Heraeus AG) to clear the tissue debris, and then the supernatant was further centrifuged at 100000*g* for 1 h at 4 °C to separate the soluble (supernatant) and membrane-associated proteins (pellet). To extract the membrane-associated proteins, the pellet was homogenized in 250 μL of high-KCl buffer containing 1% Triton X-100 and once again centrifuged at 100000*g*. The resultant supernatant was used as the detergent-extracted fraction of the membrane pellet for all the pull-down experiments.

Immunoprecipitation and MT Pull-Down Studies. For the immunoprecipitation experiment, the fly heads were extracted in HNME buffer [20 mM HEPES (pH 7.4), 150 mM NaCl, 5 mM $MgSO_4$, 5 mM EGTA, 0.1% Triton X-100, 1 mM PMSF, and protease inhibitor cocktail] in the same manner described above, and the remaining procedure was followed as per the earlier description (*14*). The microtubule pull-down method is adapted from an earlier report (*2*). Briefly,

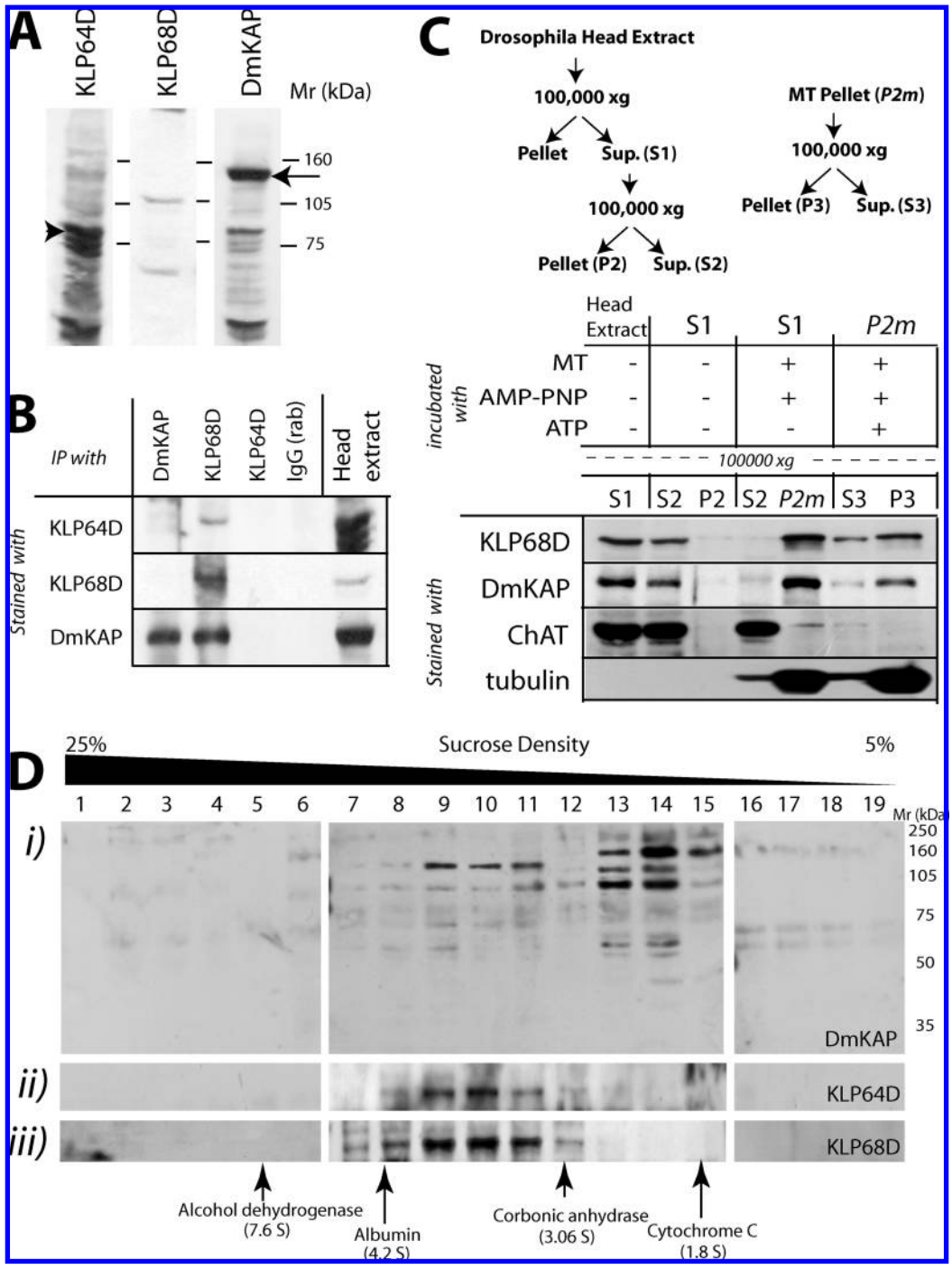

FIGURE 1: DmKAP is part of functional kinesin-2 complex in *Drosophila*. (A) Western blots of the soluble fly head extract separately stained with MAbKLP64D, anti-KLP68D, and MAbDmKAP. The arrowhead indicates the ~86 kDa KLP64D positive band, and the arrow indicates the ~120 kDa DmKAP positive band as expected from the predicted amino acid compositions of the respective polypeptides. (B) Western blots of immunoprecipitated products of the head extract were separately stained with KLP64D, KLP68D, and DmKAP specific antisera as marked in the figure. An aliquot of the head extract used for the study was loaded in the rightmost lane for comparison. The purified rabbit anti-KLP68D coprecipitated both the 86 kDa KLP64D and 120 kDa DmKAP bands, while MAbDmKAP could only precipitate DmKAP. MAbKLP64D failed to precipitate any of the three. This indicates that MAbDmKAP disrupts the complex and the KLP64D epitope is inaccessible in the native form. (C) MT association of the kinesin-2 subunits from the fly head extracts was tested by the standard technique as discussed in Materials and Methods. S1, S2, and S3 are sequential supernatant fractions collected at successive stages of ultracentrifugation, while P2 and P3 are the pellet fractions as indicated in the flowchart at the top of the panel. The supernatants and the pellets were incubated with the buffer, MT, and AMP-PNP as indicated in the table in the middle part of the panel. An aliquot from each step was separated via SDS−PAGE and transferred to a PVDF membrane, which was immunostained with specific antisera as indicated in the left margin at the bottom part of the panel. This revealed that the 120 kDa DmKAP along with the 105 kDa KLP68D are pulled down with the MT in the presence of 4 mM AMP-PNP, and they are partly released from the MT in the presence of additional 10 mM ATP. A small fraction of the soluble ChAT, a known cargo of the kinesin-2 complex in axons, was also associated with the MT along with the motor subunits. (D) Western blots of the 25 to 5% sucrose density gradient sedimentation fractions of the wild-type *Drosophila* head extracts were separately immunostained with the (i) DmKAP, (ii) KLP64D, and (iii) KLP68D specific antisera. The 120 kDa DmKAP, 86 kDa KLP64D, and 105 kDa KLP68D bands were found to cosediment in fractions 9−11. Two additional forms of DmKAP (M_r = 130 and 102 kDa) were found in fractions 13−15, which did not contain the motor subunits. The molecular sizes of the immunostained bands were estimated with respect to the migration of the Rainbow Markers (Amersham Pharmacia Ltd.) in the Western blots.

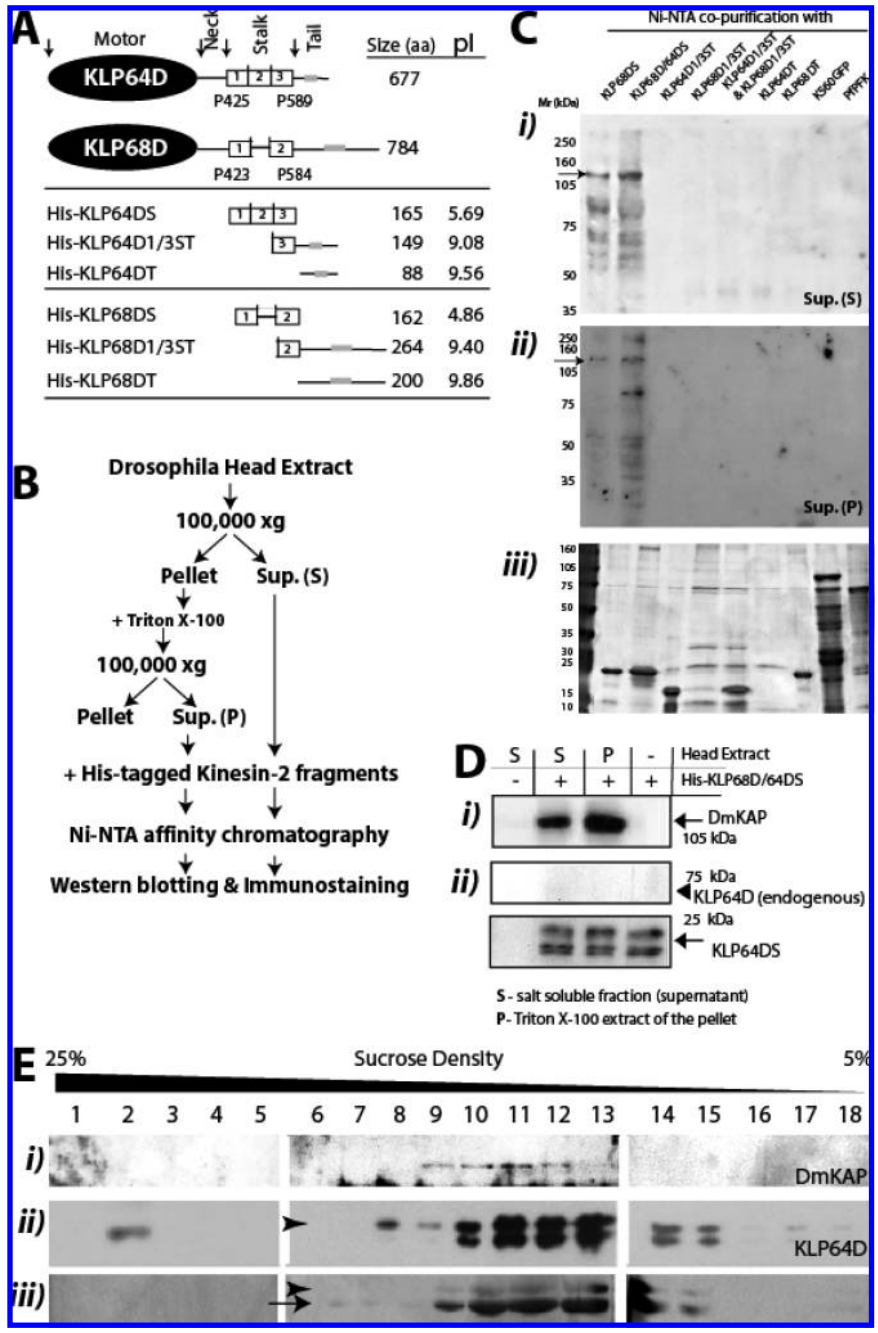

FIGURE 2: Identification of the DmKAP interacting domains on the kinesin-2 motor subunits. (A) The domain organization of the kinesin-2 motor subunits, KLP64D and KLP68D, with their relative amino acid lengths is shown. Positions of the predicted coiled-coil (cc) motifs are indicated by white boxes with numerals, and key residues marking the limits of the stalk (S) domains are indicated at appropriate positions in the figure. The tail (T) domains at the C-termini are dissimilar in length, but both contained a small stretch of conserved residues in the middle (gray boxes; also see Figure 1 of the Supporting Information for details). The table in the bottom panel includes the names and relative maps of the recombinant fragments used in this study. The N-termini are always oriented at the left, and the corresponding amino acid lengths as well as the predicted pI values of the respective fragments are indicated at the right. (B) Flow diagram illustrating the copurification and identification strategy from the cell free extracts of adult *Drosophila* heads. Aliquots (100 μL) of the 100000*g* supernatant (sup) and the detergent-extracted fraction of the pellet (P) of the fly head homogenate were separately mixed with equal molar amounts (~0.4 nmol) of the purified recombinant kinesin-2 fragments and then passed through Ni-NTA beads. The proteins bound to Ni-NTA beads were eluted with 300 mM imidazole, separated via 10% SDS−PAGE, transferred to a PVDF membrane, and stained with MAbDmKAP. (C) MAbDmKAP staining of the Western blots shows expected size bands (arrows, i and ii) in the lanes containing fractions eluted with His-KLP68DS and heterodimeric His-KLP68D/64DS. (iii) Coomassie-stained SDS−PAGE gel loaded like the ones used for making the Western blots that indicate the relative levels of the recombinant proteins in each lane. His-K560GFP and His-*Pf*PFK were used as negative controls. (D) Ni-NTA eluates of the head extracts mixed with purified His-KLP68D/64DS were Western blotted and stained with the MAbDmKAP (i) and MAbKLP64D (ii). These show prominent DmKAP (arrow, i) as well as His-KLP64DS (arrow, ii) bands, but there was no endogenous KLP64D band (arrowhead, ii). (E) Ni-NTA eluate of the His-KLP64D/68DS and head extract mixture separated on sucrose density gradient and Western blots of the fractions immunostained with MAbDmKAP (i) and MAbKLP64D (ii). (iii) An equivalent set of SDS−PAGE gels were silver stained to reveal the positions of the His-KLP64DS (arrowhead) and KLP68D (arrow) bands. Endogenous DmKAP (i) is found to cosediment with His-KLP64D/68DS between fractions 9 and 12. MAbKLP64D was always found to stain two closely migrating bands of KLP64DS in the lanes containing His-KLP64D/68DS, and the arrowhead in panel ii indicates the expected position of the His-KLP64DS band.

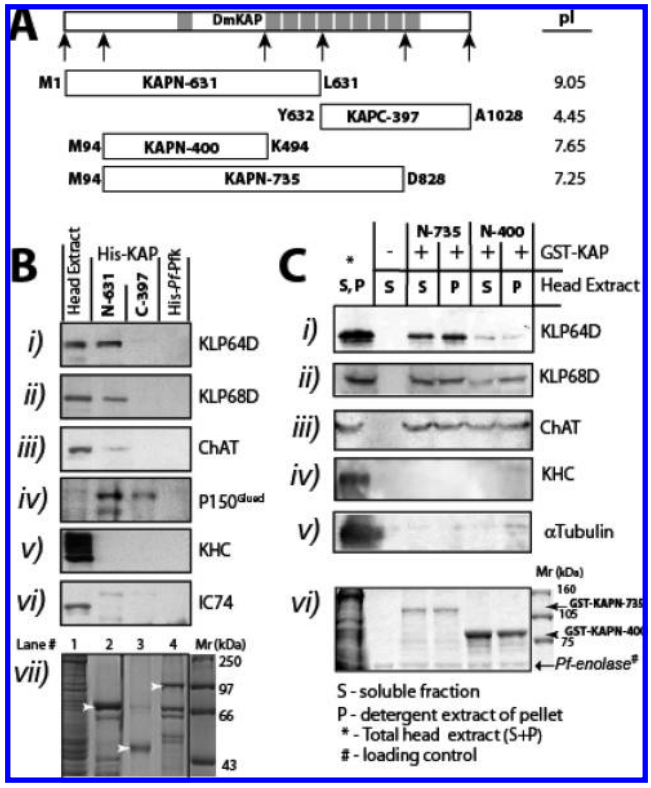

FIGURE 3: N-Terminal part of DmKAP that binds to the endogenous kinesin-2 motor subunits. (A) Schematic illustrating the relative distribution of the predicted ARMs (gray boxes) in the DmKAP sequence. Vertical arrows indicate the amino acid positions at the start and at the ends of different recombinant fragments that were cloned and expressed in *E. coli*. For each fragment, the first and last amino acid along with their position in the endogenous DmKAP sequence are mentioned in the appropriate margins. The pI values of the respective DmKAP fragments are given at the right. (B) Equal amounts (100 μL) of fly head extract were separately mixed with ~0.4 nmol of purified His-KAPN-631, His-KAPC-397, and His-*Pf*PFK along with the Ni-NTA beads. After several washes, the bead eluates were analyzed by immunostaining the Western blots with different antisera (i−vi), and a separate set was visualized by Coomassie staining after SDS−PAGE (vii). White arrowheads in panel vii indicate the expected positions of recombinant His-KAPN-631, His-KAPC-397, and His-*Pf*PFK in the respective lanes of the gel. (C) A similar copurification experiment was conducted with GST-KAPN-735 and GST-KAPN-400. Western blots of the glutathione Sepharose bead eluates were analyzed by immunostaining with different antisera (i−v). Both GST-KAPN-735 and GST-KAPN-400 could pull down KLP64D, KLP68D, and ChAT but not KHC and tubulin. A similar set was separated via SDS−PAGE and visualized by Coomassie staining of the gel (vi). Equal amounts of recombinant His-*Pf*enolase (fine arrow, vi) were mixed with the eluates before being loaded to assess loading variations.

1500 fly heads were extracted in 3 mL of PME [35 mM PIPES (pH 6.9), 5 mM $MgSO_4$, 1 mM EGTA, 0.5 mM EDTA, 1 mM PMSF, and 1 mM DTT] containing protease inhibitor cocktail. Then 200 μL portions of the first 100000*g* supernatant (S1) were mixed either with PME (sham) or with 4 mM AMP-PNP, 20 μM Taxol (Sigma Chemical Co., St. Louis, MO), and 1 mM GTP along with 1 mg/mL purified goat MT, incubated at 30 °C for 30 min, and centrifuged at 22 °C for 30 min at 100000*g*. Each pellet (P2) was dissolved in 200 μL of PME and assessed by immunostaining of the Western blots along with the corresponding supernatants (S2). For the ATP dependent release assay, a separate P2 obtained from S1 incubated with AMP-PNP and MT was resuspended in 200 μL of PME containing 10 mM ATP, 20 μM Taxol, and 1 mM GTP and incubated at 30 °C for 30 min. It was further centrifuged at 100000*g* as described previously, and the resultant pellet (P3) was again dissolved in 200 μL of PME for assessment by Western blotting and immunostaining along with S3.

Sucrose Density Gradient Sedimentation. Sucrose solutions (5 and 25%) were made in high-KCl buffer [19 mM KH_2PO_4, 81 mM K_2HPO_4, 400 mM KCl, and 1 mM DTT (pH 7.4)] containing protease inhibitor cocktail (Roche GmBH). Five milliliters of a continuous gradient (25% at the bottom to 5% at the top) was prepared in a SW50.1 ultracentrifuge tube (Beckman Coulter Inc.) by using a homemade gradient maker and peristaltic pump (GE Healthcare Ltd.); 200 μL of the soluble fly head extract was laid on the top of the gradient and then centrifuged at 150000*g* for 24 h at 4 °C by using a SW50.1 (swing bucket) rotor in an Optima LE80K (Beckman Coulter Inc.) ultracentrifuge. Following this, 18 equal size (~300 μL) fractions were collected by gentle aspiration from the bottom and analyzed by immunostaining.

Affinity Copurification of Native and Recombinant Drosophila Proteins. Aliquots (100 μL) of the soluble and detergent-extracted fractions of the *Drosophila* head homogenates were separately mixed with fixed amounts of purified recombinant proteins in high-KCl buffer. The mixtures containing the His-tagged recombinant proteins were incubated with 100 μL of Ni-NTA agarose beads, and those containing GST-tagged recombinant proteins were incubated with an equal amount of glutathione Sepharose beads for 2 h at 4 °C. Following this, the Ni-NTA beads were washed with several changes of ice-cold high-KCl buffer containing 20 mM imidazole and the glutathione Sepharose beads with the same buffer containing 0.1 mM glutathione. Finally, the bound proteins were eluted by incubating the beads in 100 μL portions of high-KCl buffer containing 300 mM imidazole (for the Ni-NTA beads) or 1 mM glutathione (for the glutathione Sepharose beads). For serial affinity purifications of the recombinant proteins, 10 mL portions of bacterial cell extracts in TMN-D containing different His- and GST-tagged recombinant proteins were mixed together with 0.5 mL of Ni-NTA beads and incubated for 2 h on ice. The beads were then washed and eluted with equal bead volumes of TMN-D containing 300 mM imidazole using the procedure described above; 0.3 mL of the eluted fractions was further incubated with 0.3 mL of glutathione Sepharose beads and washed and eluted with equal bed volumes of TMN-D containing 1 mM glutathione. The buffer conditions and salt concentrations were kept constant throughout this process. A similar serial purification was performed in reverse order and under the same buffer conditions but at different salt concentrations as indicated in Results.

Western Blots and Immunostaining Techniques. The protein mixtures were separated via SDS−PAGE and transferred to PVDF membrane (Hybond-P, Amersham Biosciences Plc.) following the supplier's protocol and incubated in different primary antiserum solutions in 20 mM Tris-buffered saline (TBS, pH 7.4) containing 0.1% Tween 20 according to the dilutions listed in Table 2 of the Supporting Information. Subsequently, they were incubated either in rabbit anti-mouse-HRP (dilution, 1:20000; Sigma Chemical Co.) or in goat anti-rabbit-HRP (dilution, 1:20000; Sigma Chemical Co.) in TBS-T and developed by using an ECL chemiluminescence detection kit (GE Healthcare Ltd.).

Antibodies. All the antisera and their respective dilutions used in the course of this study are listed in Table 2 of the Supporting Information. The custom monoclonal antibodies specific to the KLP64D stalk (KLP64DS) and the N-terminal fragment of DmKAP (KAPN-400) were raised by immunizing female mice with purified His-KLP68D/64DS and GST-KAPN-735, respectively. They were produced and supplied by BioKlone Ltd. (Chennai, India). The clones were selected by subtractive ELISA screenings. At the first stage, the clones that cross reacted to unrelated proteins His-*Pf*PFK and GST were eliminated. The remaining clones were then tested for reactivity to purified His-KLP68D/64DS and His-KLP68DS (for selecting the MAbKLP64D), or to GST-KAPN-400 (for selecting the MAbDmKAP). Finally, they were confirmed by immunostaining the Western blots of the purified antigens as well as the adult *Drosophila* head extracts. The monoclonal antibodies selected for this study were further screened by immunostaining the Western blots of *Drosophila* head extracts. A detailed description of the generation and characterization of these monoclonal antibodies is under preparation, and it will be reported shortly. A polyclonal antibody against the stalk tail fragment of KLP68D was raised in rabbits and purified using the recombinant KLP68D stalk tail fragment as described in ref *12*.

Distant Homology Modeling of the Stalk Domains of Kinesin-2 Motor Subunits and KAP. The sequences of KLP64D (AAF50786) and KLP68D (AAA50008) were obtained from the Entrez database. The coiled-coil regions were predicted using PAIRCOIL (http://groups.csail.mit.edu/cb/paircoil/cgi-bin/paircoil.cgi) (*23*) and reaffirmed through Phyre 0.2 (http://www.sbg.bio.ic.ac.uk/phyre) (*24*). The crystal structure of the pig tropomyosin homodimer (entry 1C1G) (*25*) was obtained from the Protein Data Bank (PDB). A and B chains of 1C1G were simultaneously employed as templates to build the heterodimeric stalk model of KLP64D and KLP68D (17.6 and 18.8% identical, respectively) by using MODELER version 8.2 (http://www.salilab.org/modeller) (*26*). Subsequently, the generated model was subjected to "Powell" energy minimization for 3000 iterations with the Tripos force field using SYBYL version 7.1 (http://www.tripos.com). The WHAT-IF (http://swift.cmbi.ru.nl/servers) (*27*) and COILCHECK (http://caps.ncbs.res.in/coilcheck) (*28*) servers were used to analyze the geometric quality and interface region of the KLP64D/68DS heterodimer. Similar homodimeric models of the KLP64D and KLP68D stalks were generated for comparisons. The stabilization energy (ΔSE) was calculated as the free energy change (ΔG) due to dimerization after the energy minimization according to the following equation:

$$\Delta SE = E_T - \sum_{i=1}^{2} E_i$$

where E_T is the total free energy of the dimer and E_i is the free energy of subunit i.

An identical exercise was performed with the MmKIF3A (NP_032469) and MmKIF3B (NP_032470) sequences to yield the MmKIF3A/BS model. The DmKAP sequence (NP_727512) was obtained from Entrez and aligned with other KAP sequences from different phyla by using CLUSTAL version 2.0.8 (Figure 2 of the Supporting Information). Fold predictions were obtained by using Phyre 0.2 and the PURE server (http://caps.ncbs.res.in/PURE) (*29*). A model structure of the DmKAP fragment between the E409 and I883 residues was built on the basis of the template structure of β-catenin (PDB entry 1JDH, chain ID A) as described above. Subsequently, the generated model was subjected to Powell energy minimization for 3000 iterations with the Tripos force field using SYBYL version 7.1. An identical exercise was performed with the MmKAP3A (P70188) sequences to yield the MmKAP3A model.

Modeling the Heterotrimeric Complex. The KLP64D/68DS model was docked to the DmKAP model by using GRAMM 1.03 (http://vakser.bioinformatics.ku.edu/resources/gramm/gramm1). It was particularly suitable in our case, as it allows inputs of low-resolution structures. We used the low-resolution generic docking with a grid step of 6.5 Å and a grid size of 64 Å. The ligand was rotated at 10° intervals. The energy score for repulsion was 10, and the energy score for attraction was 0. The 20 docked structures, among the top 1000 best score matches, were selected and analyzed using WHATIF (http://bioportal.weizmann.ac.il/oca-bin/lpccsu) and CSU (http://bip.weizmann.ac.il/oca-bin/lpccsu) servers. Once again, the models were subjected to Powell energy minimization as before by using SYBYL version 7.1, and the best docked model was selected on the basis of the lowest calculated free energy (ΔG) and the highest numbers of probable salt bridges, hydrophobic interactions, and hydrogen bonds between the subunits. The MmKIF3A/BS and MmKAP3A models were also docked in the same manner to yield an independent MmKAP3A−KIF3A/BS model. To further test the specificity of the DmKAP−KLP64D/68DS model, sets of amino acid residues in the DmKAP sequence, predicted to interact with KLP64D/68DS in the model, were replaced with alanine (A), and the resultant models of the mutant DmKAP sequences were docked to the wild-type KLP64D/68DS model as per the procedure described above.

RESULTS

KLP64D, KLP68D, and DmKAP Sediment Together at High Ionic Concentrations. The *Drosophila* kinesin-2 subunits were previously immunoprecipitated together with the ChAT and AChE from the adult head extracts (*14*). Since new monoclonal antibodies were generated against the N-terminal fragment of DmKAP and the KLP64DS for this study, we decided to reconfirm the previous results with the new reagents. MAbKLP64D stained three bands between 86 and 70 kDa (arrowhead, Figure 1A), and MAbDmKAP stained a prominent band at 120 kDa (arrow, Figure 1A) in the soluble head extracts. Purified anti-KLP68D stained two bands at 105 kDa and below 75 kDa (Figure 1A). The 86 kDa KLP64D band along with the 105 kDa KLP68D and the 120 kDa DmKAP bands were coprecipitated with anti-KLP68D (Figure 1B). MAbDmKAP could only precipitate the endogenous DmKAP, while MAbKLP64D failed to precipitate even the endogenous KLP64D (Figure 1B). All these confirmed that MAbDmKAP and MAbKLP64D recognized the respective proteins in Western blots, and *Drosophila* kinesin-2 is a heterotrimeric complex consisting of KLP64D, KLP68D, and DmKAP as suggested by the co-immunoprecipitation by anti-KLP68D (Figure 1B) as well as our earlier study (*14*). The co-immunoprecipitation results

also suggested that the epitopes recognized by MAbDmKAP and the MAbKLP64D are inaccessible in the kinesin-2 complex in solution. A further MT sedimentation assay was carried out to confirm that DmKAP is part of the functional kinesin-2 complex. As expected, most of the DmKAP along with the KLP68D was associated with the MT pellet in the presence of 4 mM AMP-PNP, and they were partly released in presence of 10 mM ATP (Figure 1C). In contrast, only a small fraction of the soluble ChAT was associated the MT pellet. Altogether, these results indicated that DmKAP is an integral part of the kinesin-2 complex in *Drosophila*. The ChAT pull-down data are also consistent with our previous observation (*14*), and they further suggested that only a small part of the total soluble ChAT is likely to be actively transported by the motor.

To further test the stability of this complex at high salt concentrations, we studied the sedimentation pattern on the sucrose density gradient made in 400 mM KCl. This revealed that 120 kDa DmKAP sediments together with 86 kDa KLP64D and 105 kDa KLP68D (Figure 1D). Two other forms of DmKAP (~130 and 102 kDa) were found to sediment separately behind the kinesin-2 complex (Figure 1D, i). The *DmKap* gene is predicted to encode five different mRNAs and three different proteins by genome annotations. Earlier studies also showed that tyrosine residues in the C-terminal half of the human KAP3A are phosphorylated by the breast tumor kinase, thereby altering the mobility of the protein on SDS−PAGE (*30*). Therefore, a combination of these could account for the other forms of DmKAP, which sediment separately from the motor subunit. Nevertheless, the data further helped to establish that the *Drosophila* kinesin-2 is stable at high ionic concentrations and it is composed of three unique subunits as recognized by the antibodies.

Both Heterodimeric KLP64D/68D and the KLP68D Stalk Fragments Pulled Down 120 kDa Endogenous DmKAP. Both KLP64D and KLP68D are predicted to contain conserved kinesin-like motor (M) domains at the N-termini, ~160-amino acid stalk (S) domains in the middle, and globular tail (T) domains of dissimilar lengths at the C-termini (Figure 2A). The limits of the S domains are determined by proline residues in both polypeptides (Figure 1 of the Supporting Information). KLP64DS is predicted to have three coiled-coil motifs [cc-1, -2, and -3 (Figure 1 of the Supporting Information)] of nearly equal lengths interspersed with short random coils (stutters), whereas only two such motifs were predicted at the N- and C-terminal ends of the KLP68DS sequence [cc-1 and -2 (Figure 1 of the Supporting Information)] with a gap in the middle. Thus, both KLP64DS and KLP68DS are divided into three equal parts (Figure 2A). The KLP64DT and KLP68DT sequences are dissimilar, and apart from a small conserved region in the middle (gray boxes, Figure 2A), the rest of the tails are poorly conserved (Figure 1 of the Supporting Information). In addition, the stalk domains are predicted to have low isoelectric point (pI) values; those for the tails are higher (Figure 2A).

To determine the DmKAP binding regions on the motor subunits, recombinant KLP64D and KLP68D fragments containing N-terminal His tags (Figure 2A) were expressed in bacteria (Table 1 of the Supporting Information). Except for His-KLP64DS, all the other His-tagged recombinant proteins were soluble, and they were purified by using Ni-NTA chromatography. His-KLP64DS mostly precipitated with the high-speed pellet, although both His-KLP68D/64DS and His-KLP64D/68DS were soluble. Therefore, we excluded His-KLP64DS from the experiment. Each of the recombinant proteins was tested for its ability to pull down the endogenous DmKAP from the fly head extracts by Ni-NTA affinity chromatography. For this, approximately 0.4 nmol of the affinity-purified recombinant protein was independently mixed with the 100000*g* supernatant (sup) as well as with the detergent extract of the pellet (P) of the high-KCl fly head extracts in separate tubes, and the mixtures were purified by Ni-NTA affinity chromatography (Figure 2B). The presence or absence of the endogenous DmKAP in the bead eluates was determined by immunostaining the Western blots (Figure 2C), in accordance with the current belief the recombinant fragments containing the tail (T) domains were expected to retain DmKAP on the Ni-NTA beads by this procedure.

To our surprise, only His-KLP68DS and His-KLP68D/64DS retained the endogenous DmKAP (Figure 2C). His-K560GFP (N-560 amino acids of rat KHC fused to GFP) (*31*) and His-*Pf*PFK (His-tagged *Plasmodium falciparum* phosphofructokinase) (*32*), which were used to monitor nonspecific interactions due to the His tag, failed to pull down the endogenous protein. We also noted that the endogenous KLP64D (Figure 2D) and ChAT (unpublished data) did not copurify with His-KLP68D/64DS and DmKAP, indicating that His-KLP68D/64DS does not associate with the endogenous motor subunits or the cargo. This may suggest a specific interaction between DmKAP and the stalks. To further test the solubility of the KLP64D/68DS and DmKAP complex, the Ni-NTA eluate of the His-KLP64D/68DS mixture was separated on a sucrose density gradient. The affinity tag was added to KLP64DS to facilitate one-step affinity purification of the heterodimer. Subsequently, Western blots of the fractions were stained with MAbDmKAP and the MAbKLP64D, respectively. This revealed that DmKAP cosediments with His-KLP64D/68DS (Figure 2E), indicating that the His-KLP64D/68DS−DmKAP is stable in solution. Since the endogenous DmKAP was pulled down by the stalk fragments in the presence of 400 mM KCl as well as 1% Triton X-100, it would suggest that the accessory subunit would associate with the stalk through different types of nonionic interactions.

The N-Terminal Half of DmKAP Is Essential for Binding the Motor Subunits. Sequence alignments of DmKAP homologues from different phyla identified several conserved residues in multiple stretches [I150−R193, V262−R365, D486−I658, A671−L731, and F743−E914 (Figure 2 of the Supporting Information)], and fold prediction analysis indicated 10 probable armadillo-like repeat motifs (ARMs) in the M291−D868 stretch (Figure 3A and Figure 2 of the Supporting Information). In addition, the N-terminal 631-amino acid fragment of DmKAP (pI 9.05) is predicted to be positively charged, while the remaining 397-amino acid fragment (pI 4.45) at the C-terminus is predicted to be negatively charged (Figure 3A). Interestingly, both the KLP64D and KLP68D tail domains were predicted to be positively charged. A similar domain specific distribution of charges was observed in the sea urchin homologues, which led to the proposal that the C-terminal region of SpKAP115 could interact with the respective tail domains of SpKRP85

and SpKRP95 (*2*). Hence, to test the roles of the N- and C-terminal parts of DmKAP, recombinant His-KAPN-631 and His-KAPC-397 were cloned and expressed in bacteria, and the recombinant proteins were separately used to copurify the endogenous motor subunits by using the procedure described above. In addition, two more fragments [KAPN-735 and KAPN-400 (Figure 3A)] from the middle region of DmKAP were expressed as GST-tagged polypeptides and used to copurify the native motor subunits in a similar manner.

Surprisingly though, the kinesin-2 motor subunits along with the other known interacting partners such as ChAT and the $P150^{Glued}$ were retained by His-KAPN-631 on the Ni-NTA beads (Figure 3B), whereas His-KAPC-397 could retain only $P150^{Glued}$ (Figure 3B). To further test the specificity of these retentions, duplicate Western blots were stained with KHC and IC74 specific antisera, and the results were negative (Figure 3B). A similar experiment showed that both GST-KAPN-735 and GST-KAPN-400 could also retain the kinesin-2 motor subunits (Figure 3C). Altogether, these established that the M94−K493 (GST-KAPN-400) region of DmKAP is sufficient to bind the kinesin-2 motor subunits. However, the KLP64D and KLP68D bands were qualitatively better stained when copurified with the longer construct, indicating that the interaction between the stalk domains and DmKAP is reinforced by certain additional sequence elements present in KAPN-735. *Xenopus* $P150^{Glued}$ was shown to bind to a C-terminal fragment of XKAP in a previous report (*33*). Our results indicate that the binding site is shared between the KAPN-631 and KAPC-397 fragments, and even though KAPC-397 is capable of binding *Drosophila* $P150^{Glued}$, it is insufficient for retaining the kinesin-2 motor subunits. The copurification of ChAT along with the motor subunits and $P150^{Glued}$ further indicates that the recombinant KAP fragments are associated with an otherwise native kinesin-2 complex.

Recombinant DmKAP Fragments and KLP64D/68DS Form Stable Complexes at High Salt Concentrations in Vitro. The pull-down of endogenous kinesin-2 subunits by the recombinant KLP64DS, KLP68DS, and KAPN fragments suggested a possibility of direct interaction among these polypeptides. To test this idea, we decided to reconstitute the KAPN−KLP64D/68DS complex in vitro by using bacterially expressed polypeptides. The bacterial extracts containing untagged KAPN-631 were mixed with equal molar amounts of purified His-KLP64D/68DS, His-KLP64DT, and His-KLP68DT and then repurified by using Ni-NTA affinity chromatography. Immunostaining the Western blots of the bead eluates showed that KAPN-631 is only copurified with His-KLP64D/68DS (Figure 4A). This confirmed that the N-terminal KAP binds directly to the stalk domains. In addition, purified GST-KAPN-735 and GST-KAPN-400 were separately mixed with His-KLP68D/64DS; each of these mixtures was then purified in serial order first by using Ni-NTA affinity chromatography, and then the eluates were further purified with glutathione Sepharose (Figure 4B). Both GST-KAPN-400 and GST-KAPN-735 were retained in the Ni-NTA column in the presence of the His-KLP68DS as well as His-KLP68D/64DS (Figure 4B). Similarly, the GST-tagged KAP fragments retained His-KLP68DS as well as His-KLP68D/64DS in the glutathione Sepharose column (Figure 4B). Together, these findings confirmed that KAPN-400 is indeed sufficient for binding the stalk fragments and both the KAP fragments can bind to KLP68DS in vitro. Similar serial affinity purification was performed at different ionic concentrations with the mixture containing GST-KAPN-735 and His-KLP64D/68DS to further test the salt tolerance of the complex. It revealed that the KAPN-735−KLP64D/68DS complex could be reconstituted in vitro in the presence of 300 mM NaCl or 150 mM KCl (Figure 4C) and emphasized that nonionic interactions are likely to play a role in the assembly.

A Model Describing the Interactions in the Heterotrimeric Kinesin-2 Complex. Although the results described above provided a domain specific interaction map between DmKAP and the motor subunits, it was not sufficient for describing the interactions at the residue level. Since the structures of the kinesin-2 subunits are still unknown, we applied the distant homology modeling and molecular docking technique to predict the amino acid level interactions between DmKAP and KLP64D/68DS. The heterodimer between the KLP64DS (P425−P589) and KLP68DS (P423−P584) fragments was modeled using the tropomyosin homodimer (PDB entry 1C1G) as a template, and ΔSE calculations suggested that it would be relatively stable as compared to the individual homodimers (Table 1), which conformed to the experimental findings. Similar results were produced with the MmKIF3A (K446−D610) and MmKIF3B (R407−R571) stalk fragments (Table 1). The β-catenin (PDB entry 1JDH, chain ID A) was then used to model both the DmKAP (E409−I883) and MmKAP3A (M139−A661) fragments, and they were docked to the KLP64D/68DS and KIF3A/BS models, respectively. The best docked model showed that the DmKAP−KLP64D/68DS complex would have a calculated free energy (ΔG) of −1937.99 kcal/mol, while the ΔG for the MmKAP3A−KIF3A/BS complex would be −1917.72 kcal/mol. In addition, the DmKAP fragment was predicted to dock at the C-terminal halves of both KLP64DS and KLP68DS (Figure 5B,C) through predominantly hydrophobic interactions along with some hydrogen bonds and charge interactions (Table 2 and Table 3A of the Supporting Information). A similar set of interactions was predicted from the MmKAP3A−MmKIF3A/BS model (Figure 5D−F, Table 2, and Table 3 of the Supporting Information). Furthermore, both models indicated multiple contacts among the subunits that were spread over extended regions in all three fragments (Table 2 and Table 3A,B of the Supporting Information).

Although they were built on templates with low levels of sequence identity, the models appear to be robust. First, the predicted interactions between DmKAP and KLP64D/68DS (Figure 5A−C and Table 3A of the Supporting Information) were similar to those between MmKAP3A and KIF3A/BS (Figure 5D,E and Table 3B of the Supporting Information), though the sequences of the *Drosophila* and mouse kinesin-2 subunits are quite different (Figure 2 of the Supporting Information). Second, all the predictions derived from the model are consistent with the experimental findings reported here. Our experiments suggested that the KAPN-400 (M94−K493) fragment is sufficient to bind the stalk domain, but the pull-down efficiency improved with the KAPN-735 (M94−D828)

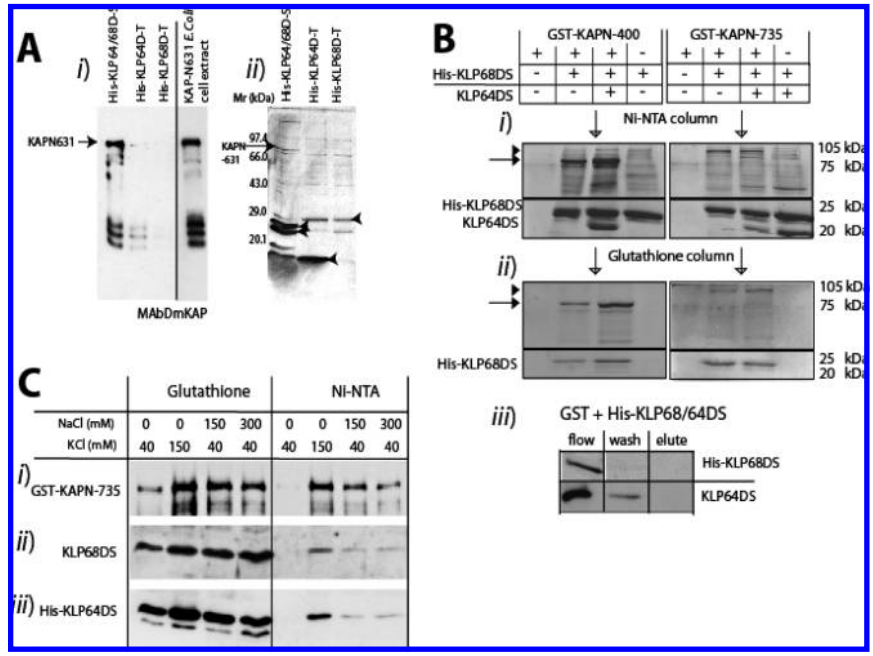

FIGURE 4: In vitro reconstitution of the DmKAP−KLP64D/68DS complex. (A) Purified His-KLP64D/68DS, His-KLP64DT, and His-KLP68DT (∼40 nmol) were separately mixed with equal volumes (0.5 mL) of the *E. coli* cell extracts expressing recombinant KAPN-631 (no tag) and 0.1 mL of Ni-NTA beads. Western blots of the bead eluates were analyzed by MAbDmKAP staining (i). The same set of eluates was separated via 8 to 15% gradient SDS−PAGE and then silver stained to reveal the positions of the recombinant proteins (ii). The arrows in panels i and ii indicate the expected positions of KAPN-631, and the arrowheads in panel ii indicate the positions of the His-tagged recombinant fragments in the respective lanes. (B) Affinity-purified GST-KAPN-735 and GST-KAPN-400 were separately mixed with His-KLP68DS as well as His-KLP68D/64DS and then purified, first by Ni-NTA affinity chromatography, and the Ni-NTA eluates were again purified by glutathione Sepharose affinity chromatography as indicated in the figure. The bead eluates from both steps were separated via SDS−PAGE and visualized via Coomassie staining (i and ii). The arrows and arrowheads indicate the positions of GST-KAPN-400 and -735, respectively. (iii) The GST and His-KLP68D/64DS mixture was passed through the glutathione Sepharose beads, and Western blots of the fractions were separately stained with anti-KLP68D and MAbKLP64D. Expectedly, His-KLP68DS and KLP64DS were found in the flow-through and wash fractions and not in the eluates, indicating that the GST tag does not interact with the recombinant kinesin-2 fragments. (C) Similar serial affinity purifications of the GST-KAPN-735−His-KLP64D/68DS complex were performed at varying salt concentrations as indicated in the top panel. The mixtures were first purified with glutathione Sepharose and then through Ni-NTA columns as indicated earlier, and the Western blots of the column eluates were immunostained with MAbDmKAP (i), anti-KLP68D (ii), and MAbKLP64D (iii). This showed that the interaction of KAPN-735 with the heterodimeric stalk remains stable even at very high ionic strengths.

Table 1: Molecular Interactions between the Stalk Domains of the Kinesin-2 Motor Subunits As Predicted from the Model Based on Tropomyosin (PDB entry 1C1G, chains A and B)

	KLP64D−KLP64D	KLP68D−KLP68D	KLP64D−KLP68D	MmKIF3A−MmKIF3A	MmKIF3B−MmKIF3B	MmKIF3A−MmKIF3B
ΔSE (kJ/mol)	−2604.34	−2550.19	−2680.47	−2287.3	−2363.14	−2655.99
no. of salt bridges (4 Å cutoff)	9	5	17	16	5	22
no. of favorable electrostatic interactions	175	154	200	248	184	214
no. of unfavorable electrostatic interactions	215	207	196	302	234	221
no. of hydrophobic interactions	48	36	46	58	50	42
no. of atomic bumps	39	37	37	64	12	35
no. of residues with bad torsion angles	4	7	2	0	0	0

fragment, implying that residues in the K493−D828 region additionally reinforce the association with the stalk domains. Although we could not model some of the N-terminal region of DmKAP found to associate with the stalk in our experiment, the docking exercise predicted that several residues in the K412−Y878 region of DmKAP could form stable contacts with KLP64DS and KLP68DS (Table 3 of the Supporting Information). To further validate these predictions, we altered the DmKAP sequences by substituting sets of the predicted interacting residues with alanine and separately docked the substituted DmKAP models to KLP64D/68DS (Figure 6). While one of the substitutions was predicted to cause moderate defects (Figure 6B), the model suggested that replacement of the 594-NLSF-597 region with 594-AASA-597 in DmKAP could both drastically alter the topography of interactions and reduce its affinity for the stalks by 4-fold (Figure 6C). In addition, multiple alanine substitutions in the K481−N489 fragment (Figure 6D) as well as in the E521−K526 and D559−E563 regions (Figure 6E) radically altered the pattern of interactions between the DmKAP and stalk domains. This is consistent with our experimental observations as all these amino acids are included in KAPN-631 but missing from KAPC-397, which failed to pull down the endogenous motor subunits. This exercise also showed that certain amino acids in the N-terminal region of DmKAP could play important roles in determining its interactions with the stalk domains and further validated the model. The modeling analysis also

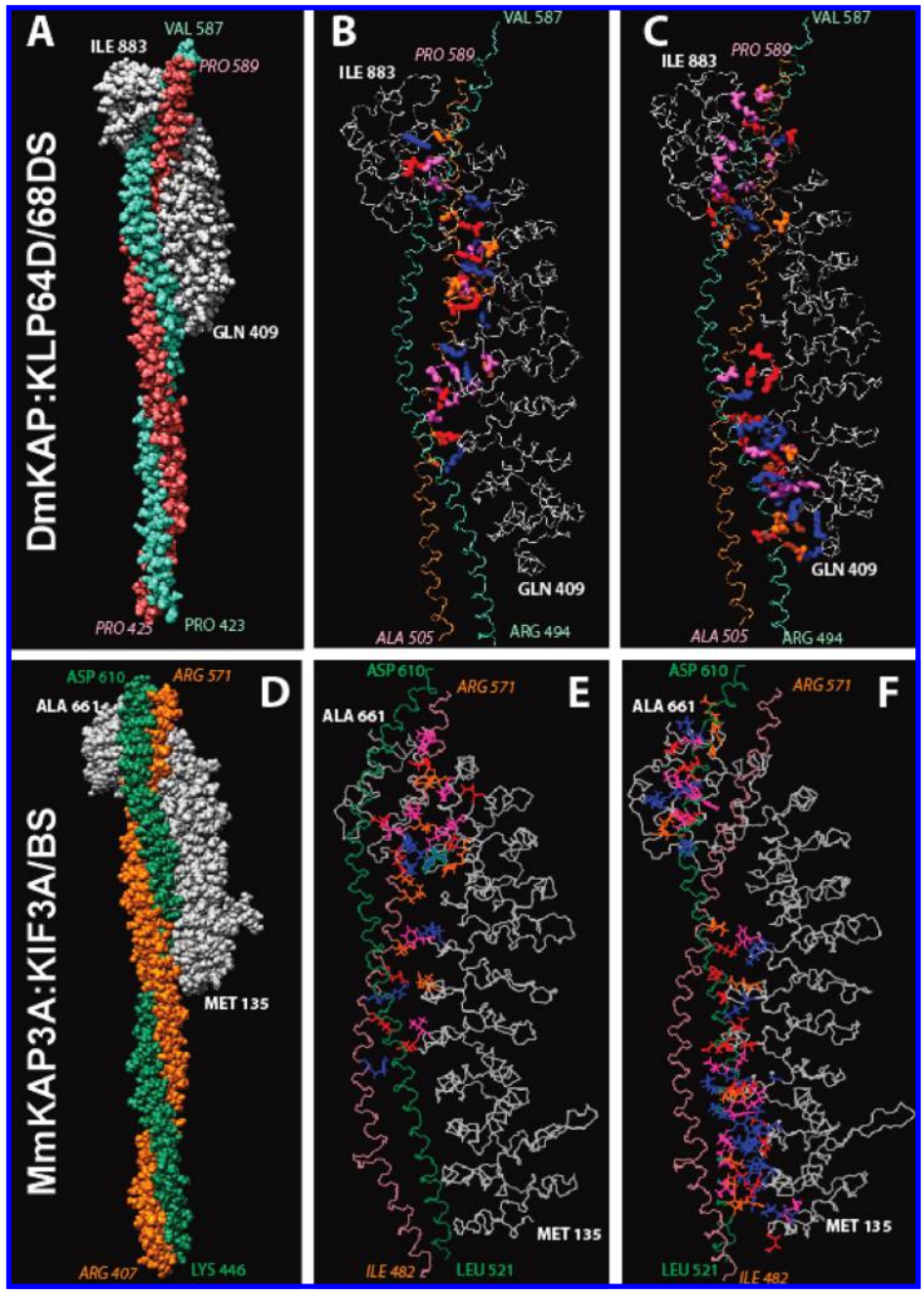

FIGURE 5: Atomic-resolution model depicting interactions in the DmKAP−KLP64D/68DS and MmKAP3A−KIF3A/BS complexes. (A) Energy-optimized DmKAP−KLP64D/68DS heterotrimer of the DmKAP (light gray), KLP68DS (aquamarine), and KLP64DS (salmon) fragments. The DmKAP fragment was modeled by using β-catenin (PDB entry 1JDH, chain A) and KLP64D/68DS by using tropomyosin (PDB entry 1C1G) as templates and docked to each other. (B and C) Backbone structures of the DmKAP, KLP64DS, and KLP68DS fragments in the DmKAP−KLP64D/68DS model. The atomic contacts between DmKAP (light gray) and KLP64DS (salmon) (B) and between DmKAP and KLP68DS (aquamarine) (C) fragments are highlighted in different colors along the chain. Amino acid residues with hydrophobic (pink), polar (orange), negatively charged (red), and positively charged (blue) side chains involved in the interactions are marked with different colors (see Table 2 and Table 3A of the Supporting Information for details). These contacts are distributed along the entire length of the protein. (D−F) Equivalent set of view for the MmKAP3A−KIF3A/BS model prepared by using an identical procedure as described above.

Table 2: Molecular Interactions between the Heterodimeric Stalk and KAP As Observed in the Model

	no. of contacts			no. of contacts		
type of interaction	KLP64D−DmKAP	KLP68D−DmKAP	total	MmKIF3A−MmKAP3A	MmKIF3B−MmKAP3A	total
hydrophobic	29	53	86	17	44	61
hydrogen bond	22	39	61	17	35	52
salt bridge (5 Å cutoff)	5	15	20	5	11	16

revealed that DmKAP is likely to occupy only one part of the KLP64D/68DS surface. This would allow other proteins to access the stalk. Similarly, only a part of the DmKAP surface was occupied by the stalk, and this would allow KAP to simultaneously bind other proteins and help to form a greater kinesin-2 complex.

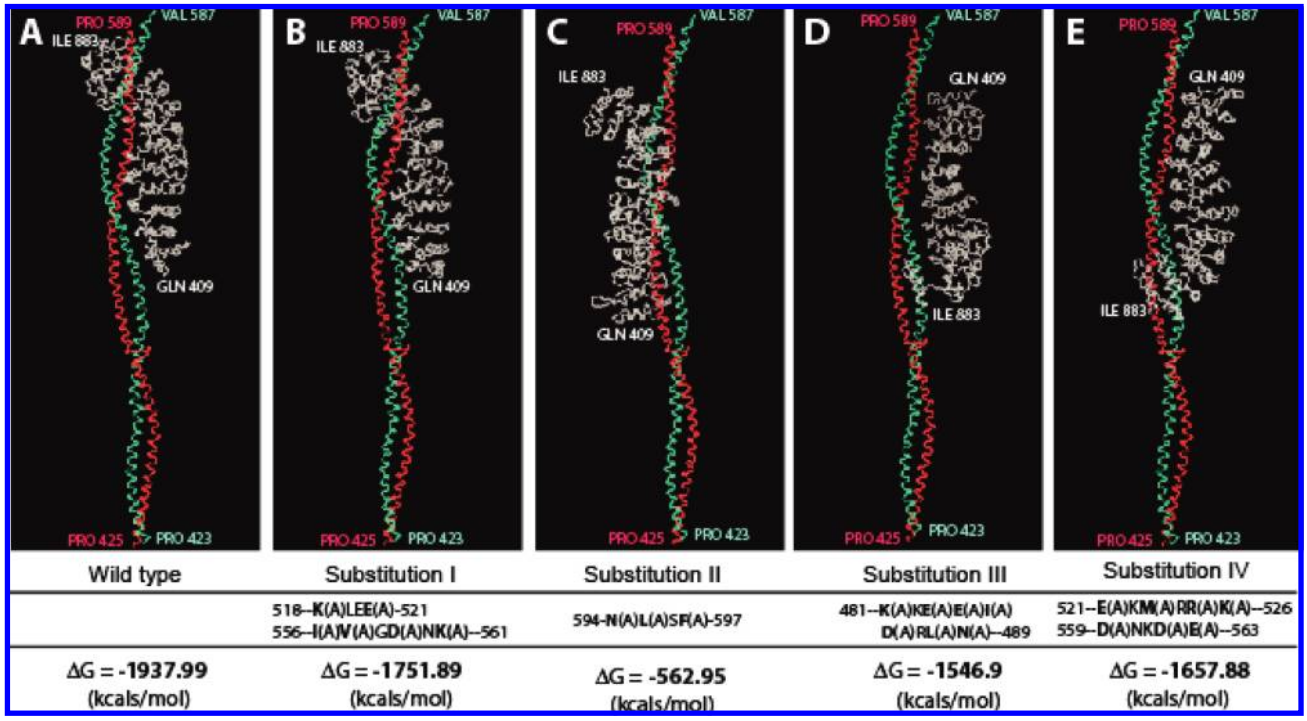

FIGURE 6: Alanine substitutions of the key interacting amino acids in DmKAP reduced the predicted affinity of interactions with KLP64D/68DS. The comparative computational docking models of the wild type (A) and substituted (B−E) DmKAP variants associated with KLP64D/68DS. Only the backbones of DmKAP (light gray), KLP68DS (aquamarine), and KLP64DS (brown) are shown to illustrate the relative positions of the subunits in the complex. The corresponding substitutions are indicated in the second row below each figure. The amino acid residues highlighted in bold letters were substituted with alanine (A) as indicated in parentheses next to them. The corresponding ΔG values as calculated from each model are indicated in the third row below the figures. The substitution I had a moderate effect on the binding, while substitutions II, III, and IV altered the topography of interactions between DmKAP and KLP64D/68DS. The free energy calculations showed that the affinity would be the lowest after substitution II.

DISCUSSION

In summary, the experimental data established two significant points underlying the basis of heterotrimeric kinesin-2 assembly. First, the affinity purification results and independent modeling exercise showed that DmKAP binds to the stalk domains of the kinesin-2 motors, and it ruled out the possibility of interaction between DmKAP and the tail domains of the motor subunits. Second, it showed that it is the N-terminal and not the C-terminal region of DmKAP that binds to the stalk domain. Computational modeling further predicted that the interactions between KAP and the motor subunits would be spread over large stretches in each subunit and certain key residues in DmKAP could be critical in maintaining its affinity for the stalk domains. Altogether, these negated an existing notion that the C-terminal part of KAP would bind to the tail domains of the kinesin-2 motor subunits and advanced a new interaction model. It will have an important impact on the current understanding of the role of the accessory protein in kinesin-2 functions. Similar models of binding between the non-motor accessory subunits and the motors have been reported for two other motor proteins. The kinesin light chain (KLC) was shown to interact with the coiled-coil stalk region of the kinesin heavy chain (KHC) subunits to constitute a 2+2 kinesin-1 complex, and this is proposed to enhance the stability of the motor (*34*). The dimeric DLC2 binds to the predicted coiled-coil stalk region of an alternatively spliced form of myosin Va (*35*), and this is shown to enhance the coiled-coil interaction between the two motor subunits (*36*). Both KLC1 and DLC2 are known to play essential roles in the respective motor functions in vivo (*35, 37*).

Originally, the kinesin-2 accessory subunit (KAP) was proposed to act as a generic cargo adapter (*18*). The addition of KAP3A to the heteromeric KIF3A/B complex was reported to have no effect in the motor activity in vitro (*38*). However, as compared to the recombinant KIF3A/B heterodimer, the heterotrimeric kinesin-2 purified from the chicken brain and the recombinant Cekinesin-2 were demonstrated to have almost 2-fold higher motility rates in vitro (*39*−*41*). Furthermore, genetic and cellular analysis in *Chlamydomonas*, *C. elegans*, and *Drosophila* suggested that the KAP subunit is essential for maintaining the kinesin-2 functions in vivo (*13, 16, 17*). The C-terminal half of KAP is the most conserved and appeared to play a vital role in the kinesin-2 functions in vivo (*16*). The role of KAP is, thus, likely to extend beyond that of a mere cargo adapter in the kinesin-2 complex. The results presented here indicate that KAP would associate along the length of the coiled-coil stalk of the motor subunits. This could further stabilize the heterodimeric coiled-coil assembly and thus improve the overall efficiency of movement such as run length. A detailed future experiment would be needed to test this prediction.

The human KAP3A homologue was also shown to interact with the adenomatosis polyposis coli (APC) (*42*), smgGDS (*43*), and human chromosome-associated protein (HCAP) (*44*) through the ARMs. In all three cases, HsKAP3A was shown to form a supercomplex along with the HsKIF3A/B heterodimer. These observations are consistent with our results and the proposed model, which shows that the motor

subunits associate with the N-terminal region of KAP while most of the predicted ARMs are at the C-terminal half of the protein. Certain other observations further indicate that KAP could glue together multiple coiled-coil motifs. XKAP was shown to interact with the $P150^{Glued}$ subunit of dynactin in *Xenopus* melanocytes and disrupt the IC74−$P150^{Glued}$ interaction (*33*). The region of $P150^{Glued}$ that binds XKAP also contained a predicted coiled-coil motif, which is involved in the interaction with the IC74 subunit of dynein (*45*). Therefore, XKAP is likely to compete for the same site on $P150^{Glued}$ as IC74. It was also shown that the $P150^{Glued}$ binding does not disrupt the XKAP−XKLP3A/B complex. *Drosophila* $P150^{Glued}$ was copurified with both the N- and C-terminal fragments of DmKAP. A careful sequence analysis indicated that the C-terminal part of KAPN-631 is homologous to the 40 amino acids of the C-XKAP fragment used in the previous study (*33*). Thus, the pull-down results are consistent with the previous report, and this further indicates that interaction between KAP and the motor subunits as well as other proteins could occur through exclusive regions. This is further supported by the proposed model, which indicates that KAP could simultaneously interact with multiple other surfaces, and this would allow it to glue together the coiled-coil stalks of the motor subunits with the other proteins. Altogether, these results suggest that KAP may act as an essential adapter to condense a supercomplex with kinesin-2 that is required for the biological activity of this motor.

The model presented here could also explain the mechanism underlying regulation of the kinesin-2 supercomplex assembly involving additional proteins. For instance, bovine IFT20, which contains a coiled-coil motif, was shown to interact with the predicted coiled-coil domain of KIF3B and IFT57 (*46*). Both IFT20 and IFT57 are part of the IFT-B complex (*46*), which is transported into the flagella by the heterotrimeric kinesin-2 complex (*5*). The KIF3B−IFT20 complex is reasonably salt tolerant, similar to the nature of interaction between DmKAP and KLP68D/64DS shown here. According to our model, both KAP and IFT20 could associate with the stalk domain on complementary surfaces, and this may define the nature of their interactions with the motor subunits. In contrast, the association of the von Hippel-Lindau tumor suppressor protein (pVHL) and KIF3A was shown to be disrupted by a recombinant KAP3A fragment, and this appeared to regulate the pVHL localization in the cell (*47*). Taken together with our results, this would indicate that pVHL and KAP3A compete for the same binding site on the stalk domains and thus regulate kinesin-2 function. This also suggests that KAP is unlikely to be the essential adaptor for all kinesin-2 cargoes as several proteins are shown to bind directly to the motor subunits. It is further supported by the observation that the synaptic nuclear envelope protein (Syne1), which is involved in cytokinesis in the NRK-1 cells, binds to the tail domain of KIF3B (*48*). Therefore, we propose that the association of KAP with the stalk could primarily regulate the kinesin-2 motor activity and could also contribute to the assembly of a greater kinesin-2 complex. This in turn could regulate the kinesin-2-mediated transports in vivo.

ACKNOWLEDGMENT

We are thankful to V. Rodrigues (Tata Institute of Fundamental Research) for supporting M.K., B. Gopal (I. I. Sc. Bangalore) for the bacterial expression vectors, and R. Mittal for introducing us to the recombinant protein work. K.R. and H.D. especially acknowledge S. Mazumdar (Tata Institute of Fundamental Research) for his continuing support and encouragement. R. Sarpal and V. Nadar prepared the GST-KAP constructs. P. Devan helped with the antibody characterization, and M. Parthiban assisted in some of the computational work. We are also thankful to the anonymous referees for their suggestions and constructive critique.

SUPPORTING INFORMATION AVAILABLE

Two figures, two PDB files containing the coordinates of the hetertromeric models, and three tables containing supplemental data. This material is available free of charge via the Internet at http://pubs.acs.org.

REFERENCES

1. Cole, D. G., Chinn, S. W., Wedaman, K. P., Hall, K., Vuong, T., and Scholey, J. M. (1993) Novel heterotrimeric kinesin-related protein purified from sea urchin eggs. *Nature 366*, 268–270.
2. Wedaman, K. P., Meyer, D. W., Rashid, D. J., Cole, D. G., and Scholey, J. M. (1996) Sequence and submolecular localization of the 115-kD accessory subunit of the heterotrimeric kinesin-II (KRP85/95) complex. *J. Cell Biol. 132*, 371–380.
3. Marszalek, J. R., and Goldstein, L. S. (2000) Understanding the functions of kinesin-II. *Biochim. Biophys. Acta 1496*, 142–150.
4. Rosenbaum, J. L., and Witman, G. B. (2002) Intraflagellar transport. *Nat. Rev. Mol. Cell Biol. 3*, 813–825.
5. Cole, D. G. (2003) The intraflagellar transport machinery of *Chlamydomonas reinhardtii*. *Traffic 4*, 435–442.
6. Nonaka, S., Tanaka, Y., Okada, Y., Takeda, S., Harada, A., Kanai, Y., Kido, M., and Hirokawa, N. (1998) Randomization of left-right asymmetry due to loss of nodal cilia generating leftward flow of extraembryonic fluid in mice lacking KIF3B motor protein. *Cell 95*, 829–837.
7. Takeda, S., Yonekawa, Y., Tanaka, Y., Okada, Y., Nonaka, S., and Hirokawa, N. (1999) Left-right asymmetry and kinesin superfamily protein KIF3A: New insights in determination of laterality and mesoderm induction by $kif3A^{-/-}$ mice analysis. *J. Cell Biol. 145*, 825–836.
8. Marszalek, J. R., Ruiz-Lozano, P., Roberts, E., Chien, K. R., and Goldstein, L. S. (1999) Situs inversus and embryonic ciliary morphogenesis defects in mouse mutants lacking the KIF3A subunit of kinesin-II. *Proc. Natl. Acad. Sci. U.S.A. 96*, 5043–5048.
9. Davenport, J. R., Watts, A. J., Roper, V. C., Croyle, M. J., van Groen, T., Wyss, J. M., Nagy, T. R., Kesterson, R. A., and Yoder, B. K. (2007) Disruption of intraflagellar transport in adult mice leads to obesity and slow-onset cystic kidney disease. *Curr. Biol. 17*, 1586–1594.
10. Lin, F., Hiesberger, T., Cordes, K., Sinclair, A. M., Goldstein, L. S., Somlo, S., and Igarashi, P. (2003) Kidney-specific inactivation of the KIF3A subunit of kinesin-II inhibits renal ciliogenesis and produces polycystic kidney disease. *Proc. Natl. Acad. Sci. U.S.A. 100*, 5286–5291.
11. Pesavento, P. A., Stewart, R. J., and Goldstein, L. S. (1994) Characterization of the KLP68D kinesin-like protein in *Drosophila*: Possible roles in axonal transport. *J. Cell Biol. 127*, 1041–1048.
12. Ray, K., Perez, S. E., Yang, Z., Xu, J., Ritchings, B. W., Steller, H., and Goldstein, L. S. (1999) Kinesin-II is required for axonal transport of choline acetyltransferase in *Drosophila*. *J. Cell Biol. 147*, 507–518.
13. Sarpal, R., Todi, S. V., Sivan-Loukianova, E., Shirolikar, S., Subramanian, N., Raff, E. C., Erickson, J. W., Ray, K., and Eberl, D. F. (2003) *Drosophila* KAP interacts with the kinesin II motor subunit KLP64D to assemble chordotonal sensory cilia, but not sperm tails. *Curr. Biol. 13*, 1687–1696.
14. Baqri, R., Charan, R., Schimmelpfeng, K., Chavan, S., and Ray, K. (2006) Kinesin-2 differentially regulates the anterograde axonal

transports of acetylcholinesterase and choline acetyltransferase in *Drosophila*. *J. Neurobiol. 66*, 378–392.

15. Kozminski, K. G., Beech, P. L., and Rosenbaum, J. L. (1995) The *Chlamydomonas* kinesin-like protein FLA10 is involved in motility associated with the flagellar membrane. *J. Cell Biol. 131*, 1517–1527.
16. Mueller, J., Perrone, C. A., Bower, R., Cole, D. G., and Porter, M. E. (2005) The FLA3 KAP subunit is required for localization of kinesin-2 to the site of flagellar assembly and processive anterograde intraflagellar transport. *Mol. Biol. Cell 16*, 1341–1354.
17. Ou, G., Koga, M., Blacque, O. E., Murayama, T., Ohshima, Y., Schafer, J. C., Li, C., Yoder, B. K., Leroux, M. R., and Scholey, J. M. (2007) Sensory ciliogenesis in *Caenorhabditis elegans*: Assignment of IFT components into distinct modules based on transport and phenotypic profiles. *Mol. Biol. Cell 18*, 1554–1569.
18. Yamazaki, H., Nakata, T., Okada, Y., and Hirokawa, N. (1996) Cloning and characterization of KAP3: A novel kinesin superfamily-associated protein of KIF3A/3B. *Proc. Natl. Acad. Sci. U.S.A. 93*, 8443–8448.
19. Yamazaki, H., Nakata, T., Okada, Y., and Hirokawa, N. (1995) KIF3A/B: A heterodimeric kinesin superfamily protein that works as a microtubule plus end-directed motor for membrane organelle transport. *J. Cell Biol. 130*, 1387–1399.
20. De Marco, V., Burkhard, P., Le Bot, N., Vernos, I., and Hoenger, A. (2001) Analysis of heterodimer formation by Xklp3A/B, a newly cloned kinesin-II from *Xenopus laevis*. *EMBO J. 20*, 3370–3379.
21. De Marco, V., De Marco, A., Goldie, K. N., Correia, J. J., and Hoenger, A. (2003) Dimerization properties of a *Xenopus laevis* kinesin-II carboxy-terminal stalk fragment. *EMBO Rep. 4*, 717–722.
22. Sambrook, J., Fritsch, E. F., and Maniatis, T., Eds. (1989) Plasmid vectors. In *Molecular Cloning: A Laboratory Manual*, 2nd ed., Cold Spring Harbor Laboratory Press, Plainview, NY.
23. Berger, B., Wilson, D. B., Wolf, E., Tonchev, T., Milla, M., and Kim, P. S. (1995) Predicting Coiled Coils by Use of Pairwise Residue Correlations. *Proc. Natl. Acad. Sci. U.S.A. 92*, 8259–8263.
24. Bennett-Lovsey, R. M., Herbert, A. D., Sternberg, M. J. E., and Kelley, L. A. (2008) Exploring the extremes of sequence/structure space with ensemble fold recognition in the program Phyre. *Proteins: Struct., Funct., Bioinf. 70*, 611–625.
25. Whitby, F. G., Jr. (2000) Crystal structure of tropomyosin at 7 Å resolution. *Proteins 38*, 49–59.
26. Eswar, N., Marti-Renom, M. A., Webb, B., Madhusudhan, M. S., Eramian, D., Shen, M., Pieper, U., and Sali, A., Eds. (2000) *Comparative Protein Structure Modeling Using Modeller*, Vol. Supplement 15, pp 5.6.1−5.6.30, John Wiley & Sons, Inc, New York.
27. Vriend, G. (1990) WHAT IF: A molecular modeling and drug design program. *J. Mol. Graphics 8*, 52–56.
28. Sowdhamini, R., Alva, V., and Syamala Devi, D. P. (2008) COILCHECK: An Interactive Server for the Analysis of Interface Regions in Coiled Coils. *Protein Pept. Lett. 15*, 33–38.
29. Reddy, C. C., Shameer, K., Offmann, B. O., and Sowdhamini, R. (2008) PURE: A webserver for the prediction of domains in unassigned regions in proteins. *BMC Bioinf. 9*, 281.
30. Lukong, K. E., and Richard, S. (2008) Breast tumor kinase BRK requires kinesin-2 subunit KAP3A in modulation of cell migration. *Cell Signalling 20*, 432–442.
31. Romberg, L., Pierce, D. W., and Vale, R. D. (1998) Role of the kinesin neck region in processive microtubule-based motility. *J. Cell Biol. 140*, 1407–1416.
32. Mehta, M., Sonawat, H. M., and Sharma, S. (2005) Malaria parasite-infected erythrocytes inhibit glucose utilization in uninfected red cells. *FEBS Lett. 579*, 6151–6158.
33. Deacon, S. W., Serpinskaya, A. S., Vaughan, P. S., Lopez Fanarraga, M., Vernos, I., Vaughan, K. T., and Gelfand, V. I. (2003) Dynactin is required for bidirectional organelle transport. *J. Cell Biol. 160*, 297–301.
34. Gauger, A. K., and Goldstein, L. S. (1993) The *Drosophila* kinesin light chain. Primary structure and interaction with kinesin heavy chain. *J. Biol. Chem. 268*, 13657–13666.
35. Puthalakath, H., Villunger, A., O'Reilly, L. A., Beaumont, J. G., Coultas, L., Cheney, R. E., Huang, D. C., and Strasser, A. (2001) Bmf: A proapoptotic BH3-only protein regulated by interaction with the myosin V actin motor complex, activated by anoikis. *Science 293*, 1829–1832.
36. Wagner, W., Fodor, E., Ginsburg, A., and Hammer, J. A., III. (2006) The binding of DYNLL2 to myosin Va requires alternatively spliced exon B and stabilizes a portion of the myosin's coiled-coil domain. *Biochemistry 45*, 11564–11577.
37. Gindhart, J. G., Jr., Desai, C. J., Beushausen, S., Zinn, K., and Goldstein, L. S. (1998) Kinesin light chains are essential for axonal transport in *Drosophila*. *J. Cell Biol. 141*, 443–454.
38. Zhang, Y., and Hancock, W. O. (2004) The two motor domains of KIF3A/B coordinate for processive motility and move at different speeds. *Biophys J. 87*, 1795–1804.
39. Berezuk, M. A., and Schroer, T. A. (2004) Fractionation and characterization of kinesin II species in vertebrate brain. *Traffic 5*, 503–513.
40. Berezuk, M. A., and Schroer, T. A. (2007) Dynactin enhances the processivity of kinesin-2. *Traffic 8*, 124–129.
41. Pan, X., Ou, G., Civelekoglu-Scholey, G., Blacque, O. E., Endres, N. F., Tao, L., Mogilner, A., Leroux, M. R., Vale, R. D., and Scholey, J. M. (2006) Mechanism of transport of IFT particles in *C. elegans* cilia by the concerted action of kinesin-II and OSM-3 motors. *J. Cell Biol. 174*, 1035–1045.
42. Jimbo, T., Kawasaki, Y., Koyama, R., Sato, R., Takada, S., Haraguchi, K., and Akiyama, T. (2002) Identification of a link between the tumour suppressor APC and the kinesin superfamily. *Nat. Cell Biol. 4*, 323–327.
43. Shimizu, K., Kawabe, H., Minami, S., Honda, T., Takaishi, K., Shirataki, H., and Takai, Y. (1996) SMAP, an Smg GDS-associating protein having arm repeats and phosphorylated by Src tyrosine kinase. *J. Biol. Chem. 271*, 27013–27017.
44. Shimizu, K., Shirataki, H., Honda, T., Minami, S., and Takai, Y. (1998) Complex formation of SMAP/KAP3, a KIF3A/B ATPase motor-associated protein, with a human chromosome-associated polypeptide. *J. Biol. Chem. 273*, 6591–6594.
45. Vaughan, K. T., and Vallee, R. B. (1995) Cytoplasmic dynein binds dynactin through a direct interaction between the intermediate chains and $p150^{Glued}$. *J. Cell Biol. 131*, 1507–1516.
46. Baker, S. A., Freeman, K., Luby-Phelps, K., Pazour, G. J., and Besharse, J. C. (2003) IFT20 links kinesin II with a mammalian intraflagellar transport complex that is conserved in motile flagella and sensory cilia. *J. Biol. Chem. 278*, 34211–34218.
47. Mans, D. A., Lolkema, M. P., van Beest, M., Daenen, L. G., Voest, E. E., and Giles, R. H. (2008) Mobility of the von Hippel-Lindau tumour suppressor protein is regulated by kinesin-2. *Exp. Cell Res. 314*, 1229–1236.
48. Fan, J., and Beck, K. A. (2004) A role for the spectrin superfamily member Syne-1 and kinesin II in cytokinesis. *J. Cell Sci. 117*, 619–629.

BI8018338